NOISY BAND SELECTION BASED ON THE INTEGRATION OF THE STACKED-AUTOENCODER AND CONVOLUTIONAL NEURAL NETWORK APPROACHES FOR HYPERSPECTRAL DATA

SELEÇÃO DE BANDAS RUIDOSAS BASEADA NA INTEGRAÇÃO DE STACKED-AUTOENCODER E REDES NEURAIS CONVOLUCIONAIS PARA DADOS HIPERESPECTRAIS

Mario Ernesto JIJÓN-PALMA[1], Caisse AMISSE[2], Jaime Carlos MACUÁCUA[3], Jorge Antonio Silva CENTENO[1]

Universidade Federal do Paraná (UFPR), Departamento de Geomática, Programa de Pós-graduação em Ciências Geodésicas, Avenida Coronel Francisco Heráclito dos Santos, 210 – Jardim das Américas – Curitiba, Paraná, Brasil.
E-mails: majijpa@hotmail.com; centeno@ufpr.br
[2]Universidade Rovuma. Avenida Josina Machel, 256, Nampula - Moçambique. E-mail: caamisse@gmail.com
[3]Universidade Eduardo Mondlane. Avenida Julius Nyerere, 3453, Maputo - Moçambique. E-mail: macua.gis@gmail.com

RESUMO - A presença de ruído em imagens hiperespectrais causa degradação e dificulta a eficiência no processamento para a classificação da cobertura terrestre. Portanto, a remoção do ruído ou a detecção automática de bandas ruidosas em imagens hiperespectrais torna-se um desafio para pesquisas na área de sensoriamento remoto. Para enfrentar esse problema, um modelo integrado (SAE-1DCNN) é apresentado nesse estudo, baseado nos algoritmos de Deep Learning conhecidos como: *Stacked-Autoencoders* (SAE) e Redes Neurais Convolucionais (CNN) para a seleção e exclusão de bandas ruidosas. O modelo proposto emprega as camadas convolucionais para melhorar o desempenho dos *Autoencoders* focados na discriminação dos dados de treinamento por meio da análise da assinatura hiperespectral do pixel. No contexto do SAE-1DCNN, as informações são comprimidas e a informação redundante é identificada e removida. Isso é possível dado à eficiência da arquitetura profunda baseada em camadas convolucionais e de agrupamento. Os resultados obtidos demonstram a capacidade do modelo em identificar automaticamente bandas ruidosas, sugerindo que a nossa abordagem tem potencial e pode representar uma alternativa promissora para a detecção de bandas ruidosas no pré-processamento de dados hiperespectrais.
Palavras-chave: Bandas ruidosas. Seleção de atributos. Redes neurais convolucionais. *Stacked-autoencoders.* Dados hiperespectrais.

ABSTRACT - The presence of noise on hyperspectral images causes degradation and hinders efficiency of processing for land cover classification. In this sense, removing noise or detecting noisy bands automatically on hyperspectral images becomes a challenge for research in remote sensing. To cope this problem, an integrated model (SAE-1DCNN) is presented in this study, based on Stacked-Autoencoders (SAE) and Convolutional Neural Networks (CNN) algorithms for the selection and exclusion of noisy bands. The proposed model employs convolutional layers to improve the performance of autoencoders focused on discriminating the training data by analyzing the hyperspectral signature of the pixel. Thus, in the SAE-1DCNN model, information can be compressed, and then redundant information can be detected and extracted by taking advantage of the efficiency of the deep architecture based on the convolutional and pooling layers. Hyperspectral data from the AVIRIS (Airborne Visible/Infrared Imaging Spectrometer) sensor were used to evaluate the performance of the proposed automatic method based on feature selection. The results showed effectiveness to identify noisy bands automatically, suggesting that the proposed methodology was found to be promising and can be an alternative to identify noisy bands within the scope of hyperspectral data pre-processing.
Keywords: Noisy bands. Feature selection. Convolutional neural network. Stacked-autoencoders. Hyperspectral data.

INTRODUCTION

The abundant and valuable spectral information captured by hyperspectral imaging through hundreds of narrow and continuous bands from the visible to the near-infrared region of the electromagnetic spectrum (0.4 to 2.5 μm), allows to recognize and distinguish very similar materials and objects on the Earth's surface (Yang et., 2018; Paoletti et., 2019; Mei et al., 2019). This

detailed spectral description of the Earth's surface has been used in different applications such as: land cover mapping (Paoletti et al., 2018; Ishida et al., 2018; Laporte-Fauret et al., 2020; Banerjee et al., 2020), mineral exploration (Carrino et al., 2018; Booysen et al., 2020; Jackisch et al., 2019), water pollution detection (Cao et al., 2021; Wei et al., 2019; Minghelli et al., 2021), among others. However, hyperspectral images suffer from degradations that can cause disruption affecting the performance of further processing. One of these degradations is noise caused by sensor instability and atmospheric interference, such as: Gaussian noise, stripe noise, impulse noise, missing lines, and mixed noise (Rasti et al., 2018; Zhang et al., 2019).

Noise identification is decisive before the analysis and interpretation of hyperspectral images considering future applications (Lu et al., 2013; Mei et al., 2019). Noisy bands can be detected and eliminated using two approaches: visual inspection and automatic selection. Visual inspection is performed by displaying each band on the screen; however, this approach is subjective and can lead to different results, even discarding useful bands (Jia et al., 2012). The automated selection approach consists of applying models, algorithms and procedures that allow computing parameters to select relevant information. Such methods use information contained in the original data to identify the noisy bands.

Noisy bands elimination resembles feature selection methods, aimed at identifying the most relevant bands from a hyperspectral set, and discarding those that are redundant or are not useful for the classification. Automated approaches for information extraction can be divided into two methods: feature selection and feature extraction (Serpico et al., 2003). According to Ettabaa and Salem (2018), feature selection has advantages over feature extraction, the main one being that it does not require any transformation to be applied to all or most of the original data with the risk of losing information when applying a transformation. According to Venkatesh and Anuradha (2019) and Zebari et al. (2020), feature selection methods based on the interaction with the learning model can be classified into: Filter (based on measurement criteria), Wrapper (based on classification accuracy metrics), Embedded (based on learning algorithms), Hybrid (based on the integration of two methods of feature selection) and Ensemble (based on the construction of a group of feature subsets).

Hyperspectral denoising techniques have evolved substantially to improve the signal/noise ratio of hyperspectral data (Rasti et al., 2018). One of these techniques is artificial intelligence based on its Machine Learning and Deep Learning models, which solve the limitation of conventional methods and show encouraging performance in the preprocessing and processing stages (Maffei et al., 2019; Paul et al., 2022). These models use features learned exclusively from data with the aim of automatically discovering an effective feature representation for a problem domain, thus avoiding the complicated and hand-crafted feature engineering process (Paul and Chaki, 2019; Yang et al., 2018). Among the most representative and widely used models in scientific works relating hyperspectral data are: Convolutional Neural Networks (CNN), Autoencoders (AE) or Stacked-Autoencoders (SAE). CNNs are supervised models, in which the convolutional layer is the basic structural unit and allow integrating spectral features with spatial contextual information on hyperspectral data in a more efficient way for feature extraction (Paoletti et al., 2019). The overall success of these networks lies mainly in the fact that the structure forces the networks to learn hierarchical contextual translation-invariant features, which are particularly useful for image categorization (Maggiori et al., 2016). AE or SAE (various stacked AE) are unsupervised symmetric neural networks that aim at learning a compressed data representation of a high-dimensional feature space with minimal information loss (Cheng et al., 2017; Audebert et al., 2019) for feature selection and, more generally, for dimensionality reduction (main application), which is useful for hyperspectral image classification, as described in Zabalza et al., 2016; Petscharnig et al., 2017; Windrim et al., 2019.

In this context, an integrated pixel-based model involving the SAE and CNN models for the selection and exclusion of noisy bands is introduced in the present study. The core of the integrated model (SAE-1DCNN) is an autoencoder that is improved by using convolutional layers in the encoding and decoding steps. This allows improving the training data discrimination through the analysis of the pixel's hyperspectral signature, taking advantage of the effectiveness of the deep architecture based on the convo-

lutional and pooling layers. To validate the proposed methodology, the results obtained were analyzed through the kappa coefficient to verify the potential of the integration of AEs and convolutional nets. Experiments were performed using different hyperspectral data sets: Indian Pines University of Pavia and Salinas, widely used by the scientific community. These obtained results demonstrated effectiveness to detect noisy bands, therefore, the proposed methodology is considered promising, solid and can be an alternative to detect noisy bands in the hyperspectral data preprocessing and avoid disturbances in subsequent analysis.

MATERIAL AND METHODS

Study Area and Dataset

To evaluate the performance of the proposed method, two hyperspectral data sets obtained by the AVIRIS (Airborne Visible/Infrared Imaging Spectrometer) sensor at different locations were used.

The datasets are Indian Pines and Salinas, which were obtained by well-known research institutions such as: Purdue University, United States. Based on the ground truth map, the labeled and collected samples for the two hyperspectral data sets were divided into training and test samples.

Of the total samples collected, 30% were used as test samples and the remaining 70% as training samples.

Indian Pines Experiment

The Indian Pines data set was captured in NW Indiana (Figure 1a). This area is covered by mixed agricultural fields with regular and irregular geometry regions. The image size is 145 × 145 pixels and the spatial resolution is 20 m. For this scene, 224 spectral bands are available, which cover the range of 0.4 to 2.5 μm wavelength with an average spectral bandwidth of 10 nm. From these bands, 34 are recognized as noisy bands due to water absorption and noise. The ground truth available in Figure 1b is divided into seven classes (Table 1), considering training and test samples of each class that were distributed throughout the full scene for land classification.
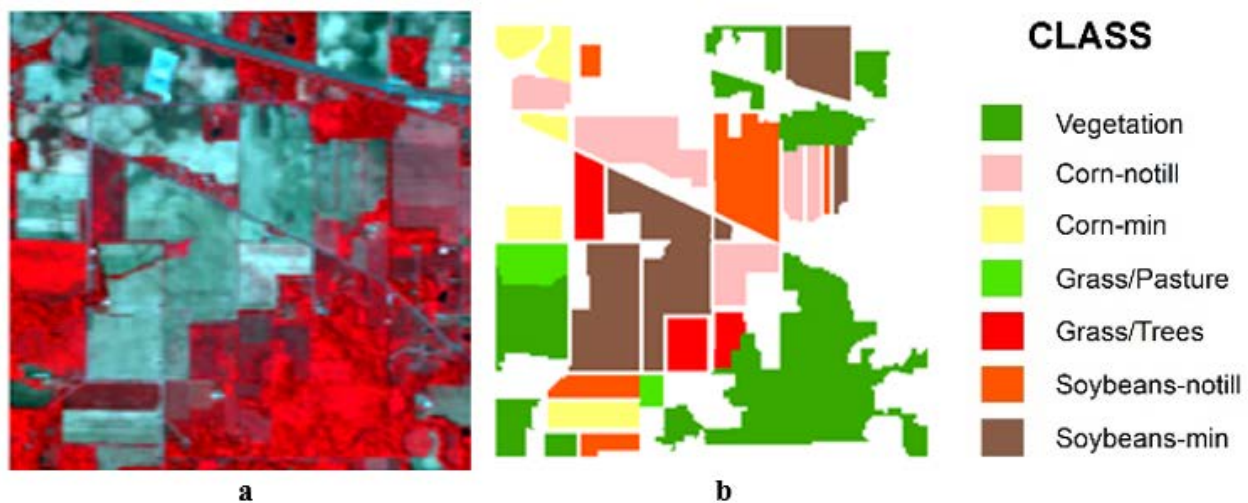

Figure 1 - (a) Hyperspectral image of the Indian Pines dataset. (b) Ground truth classification map of the Indian Pines dataset.

Table 1 - Information classes and training-test samples for the Indian Pines dataset

Class	Training	Test	Total
Vegetation	205	89	294
Corn-no till	266	127	393
Corn-min	232	111	343
Grass/Pasture	101	47	148
Grass/trees	238	106	344
Soybeans-no till	315	104	419
Soybeans-min	448	190	638

Salinas Experiment

The second hyperspectral data set was gathered over several agricultural fields of the Salinas Valley, California (Figure 2a), recording 224 spectral bands covering the range of 0.4 to 2.5 μm with 512 x 217 pixels.

The spatial resolution of this scene is 3.7 m per pixel. In this data set, as in the case of the Indian Pines data set, due to water vapor absorption, 20 noisy bands were recognized. Figure 2b shows the ground truth of this scene, which was divided into 16 classes of land cover

and its training and test samples are presented in Table 2.

Methodology

The water vapor molecules present in the atmosphere strongly absorb the emission of electromagnetic radiation, which prevents remote sensing in specific spectral regions. Since hyperspectral sensors collect data over a wide spectral range, including water absorption bands in the middle infrared, it is necessary to exclude such bands to reduce noise. In this study, noisy bands were detected and removed by two approaches: visual inspection and automated selection.
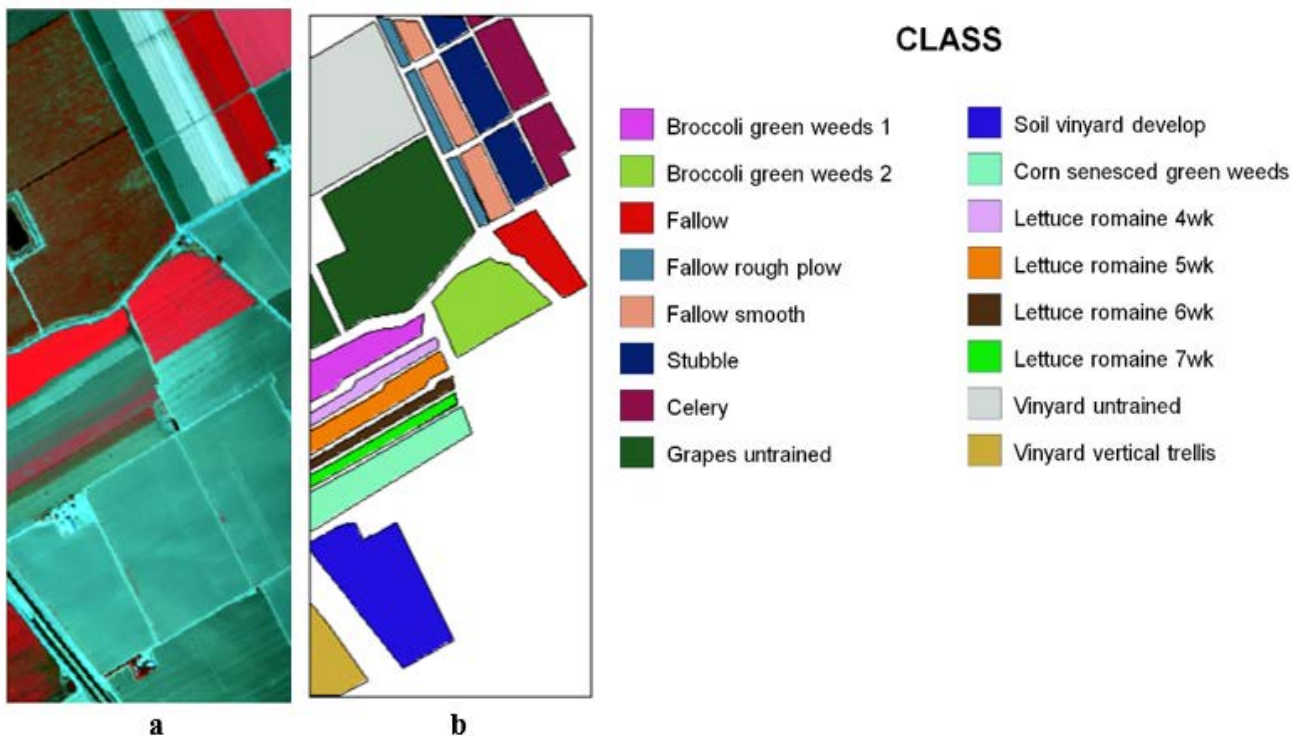

Figure 2 - (a) Hyperspectral image of the Salinas dataset. (b) Ground truth classification map of the Salinas dataset

Table 2 - Information classes and training-test samples for the Salinas dataset

Class	Training	Test	Total
Broccoli green weeds 1	1401	608	2009
Broccoli green weeds 2	2596	1130	3726
Fallow	1358	618	1976
Fallow rough plow	963	431	1394
Fallow smooth	1867	811	2678
Stubble	2754	1205	3959
Celery	2447	1132	3579
Grapes untrained	7963	3308	11271
Soil vinyard develop	4373	1830	6203
Corn senesced green weeds	2275	1003	3278
Lettuce_romaine_4wk	740	328	1068
Lettuce_romaine_5wk	1355	572	1927
Lettuce_romaine_6wk	655	261	916
Lettuce_romaine_7wk	746	324	1070
Vinyard untrained	5127	2141	7268
Vinyard vertical trellis	1270	537	1807

Exclusion of noisy bands by visual inspection

The first approach is based on visual inspection (traditional and subjective approach). For this purpose, each band of each hyperspectral set was displayed on the screen where its noise was visually evaluated, considering the exaggerated roughness produced by noise. To illustrate the effect of noise, a noisy band with water vapor interference and band without noise from the Indian Pines hyperspectral image of the AVIRIS sensor are displayed in figure 3. This is a simple method but is also affected by the user's experience, which can lead to different results. To perform this first traditional approach, all the bands composed of a hyperspectral data set were used, i.e., the AVIRIS sensor has 224 bands between noisy and noiseless bands. This result was used as reference to evaluate the second method.

Exclusion of noisy bands by automated selection

The second approach considers the SAE-1DCNN feature selection model. This proposed feature selection method is based on an integrated deep learning model that includes an SAE and convolutional networks in the encoding and decoding phases. The idea is to identify the best set of noisy variables for further classification. Therefore, the selection is guided by training samples for a restricted set of classes. Thus, the model is trained using training samples (supervised training) and then the influence of each band is analyzed, which allows identifying noisy bands. The success of the detection of noisy variables was evaluated based on the kappa coefficient of a posterior classification with the remaining bands. For this second approach, the SAE-1DCNN proposed model for feature selection was applied on a reduced set of bands, in this case, 23 bands and 32 bands were used for the Salinas and Indian Pines image, respectively. It should be mentioned that this reduced band set is composed of noisy and noiseless bands.
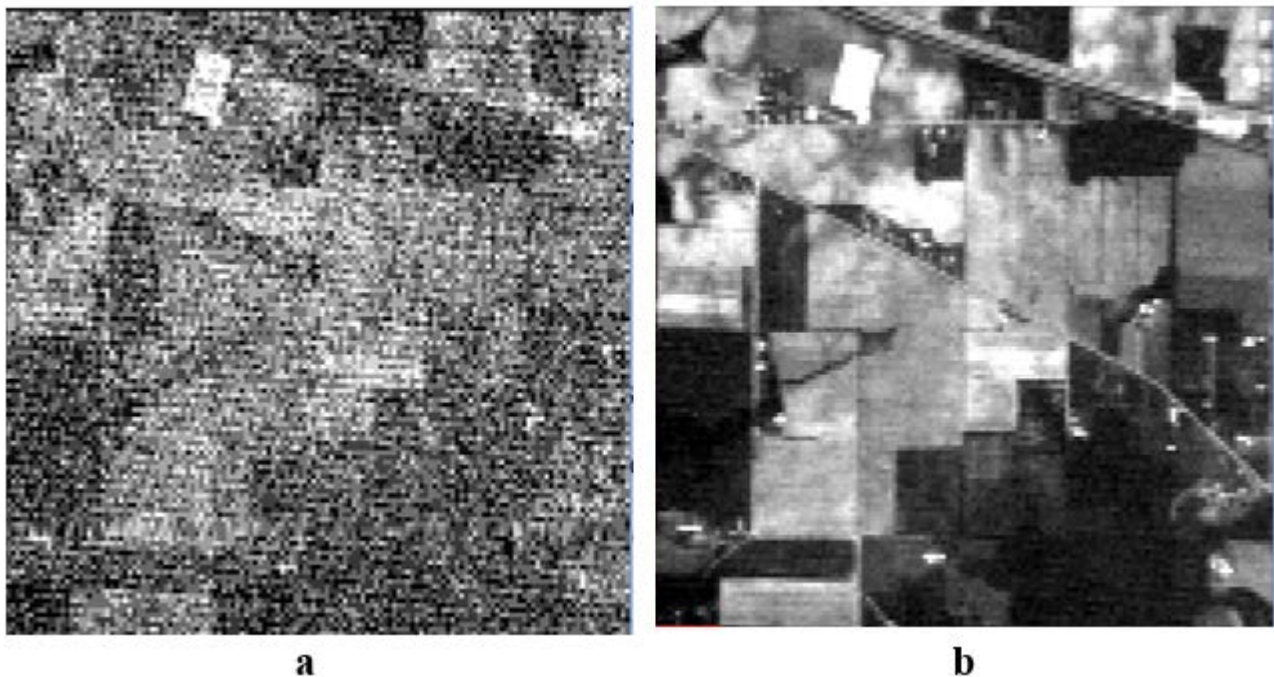

Figure 3 - Visualization of bands from the Indian Pines hyperspectral image (a) noisy band (band 103 = 1352,68 nm), (b) band without noise (band 120 = 1620,98 nm)

SAE-1DCNN model

Two different deep learning algorithms are used in the proposed SAE-1DCNN model. The first builds the base structure of the SAE-based system and the second is based on the insertion of CNNs in the encoding and decoding stages to improve the performance of this model.

In an autoencoder, during the encoding stage, an input vector $x \in R^N$ is mapped to a compact hidden representation, h, through a nonlinear activation function f. If the network has a single hidden layer, then h will be expressed by equation 1. Here, h, stands for the computed feature, f is a non-linear activation function that is applied to the weighted sum of the original data (x) using a set of weights (W). For the decoding stage, the compact representation h is used to compute the input vector as output x' using a nonlinear activation function, as in the previous stage, by equation 2.

$$h = f(Wx + b) \quad (1)$$

$$x' = f(W'h + b') \quad (2)$$

where, W is the weight matrix to be estimated at the training stage (learned), W' is the weight matrix of the reconstruction layer, b and b' are the bias vector for each stage and f is a non-linear activation function.

According to Ma et al. (2019) and LeCun et al. (2015), a CNN is a deep learning model designed to process images using the regular organization of the pixels and, it is composed of three different layers: the convolutional layer, the pooling layer, and the full connected layer. In this model the input vector is convolved with a set of K kernels with the weight matrices $W = \{W_1, W_2, \ldots, W_K\}$ and biases are added $\gamma = \{b_1, b_2, \ldots, b_K\}$, each generating a new feature map X_k, according to equation 1. The output of each convolution is modulated applying a non-linear transform $f(\cdot)$, and the same process is repeated for every convolutional layer, according to Equation 3. Figure 4 shows the structure of the proposed model based on the two stages mentioned above.

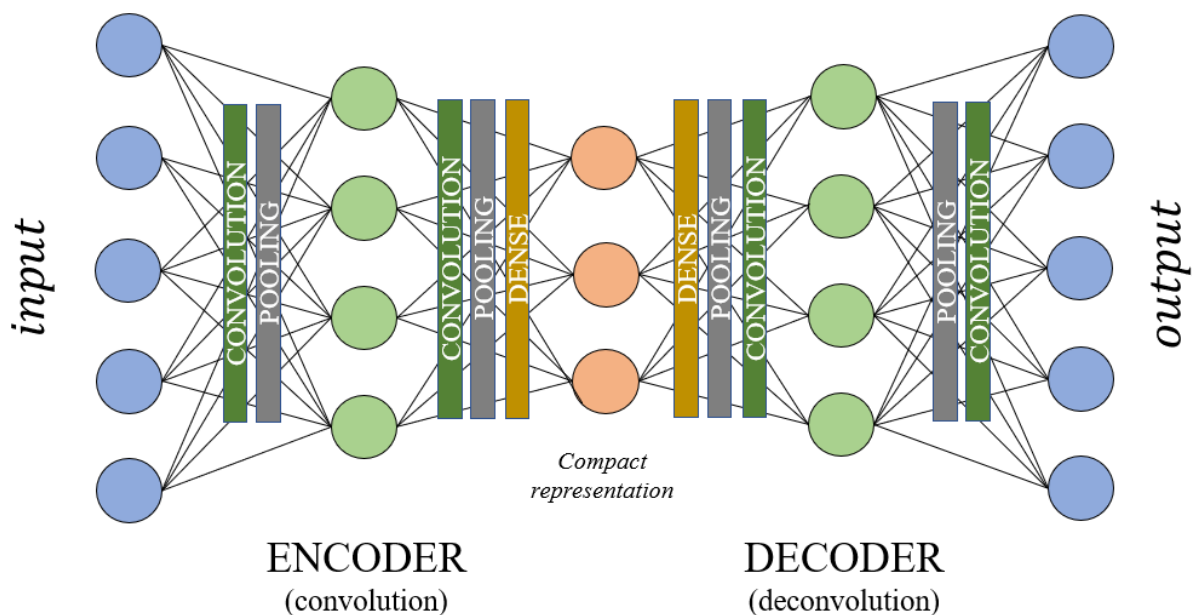$$l: X_k^l = f(W_k^{l-1} * X^{l-1} + b_k^{l-1}) \quad (3)$$

Figure 4 - Structure of the SAE-1DCNN model.

The input of the autoencoder is the original data set, the digital values in all available spectral bands. In the hidden layers, the input variables are combined, and the output is the result of the weighted sum. For this study, the autoencoder approach is applied not to detect spatial features, but to compute spectral features along the spectrum. Instead of using a moving window that slices along the image we propose the use of a one-dimensional window that slices along the bands space for each pixel. So, local spectral patterns are detected, and these patterns can be used to compute features that can help summarize the spectral signature of each pixel. To compute the output, several one-dimensional convolutional nets are applied. The purpose is to analyze the existing correlation between neighboring bands (spectral analysis) instead of the spatial correlation between neighboring pixels, as normally considered by convolutional networks.

This is possible considering that the set of hyperspectral measurements of a pixel resembles a continuous series, its spectral signature, which is characterized by local spectral variations that can be detected by a CNN. In such series, spectral signature, adjacent spectral bands are highly correlated and local variations are caused by the presence of specific elements, like water, chlorophyl or iron, for example, which introduce variations that are relative smooth. So, the complete spectral set of digital values of one pixel can also be understood as a one-dimensional function, in discrete form.

As the central idea is to replace the weighted sum of the spectral data by a convolutional net, a new value is computed from the input data applying the convolution concept to the spectral

series. This is equivalent to say that the spectral series is "filtered" using several 1D linear filters to compute the output values. The use of one-dimensional filters has the advantage that they are faster to compute than the 2D filters used in traditional convolutional layers. This significantly reduces the processing time. To improve the shape of the spectral signatures, convolutional networks are used, which describe the input vector with a reduced set of features, computed from spectral neighboring bands.

Figure 5 describes the architecture of the proposed SAE for the encoding stage (Indian Pines data set), as the SAE model is symmetric, the decoding stage is proportional to the encoding stage.
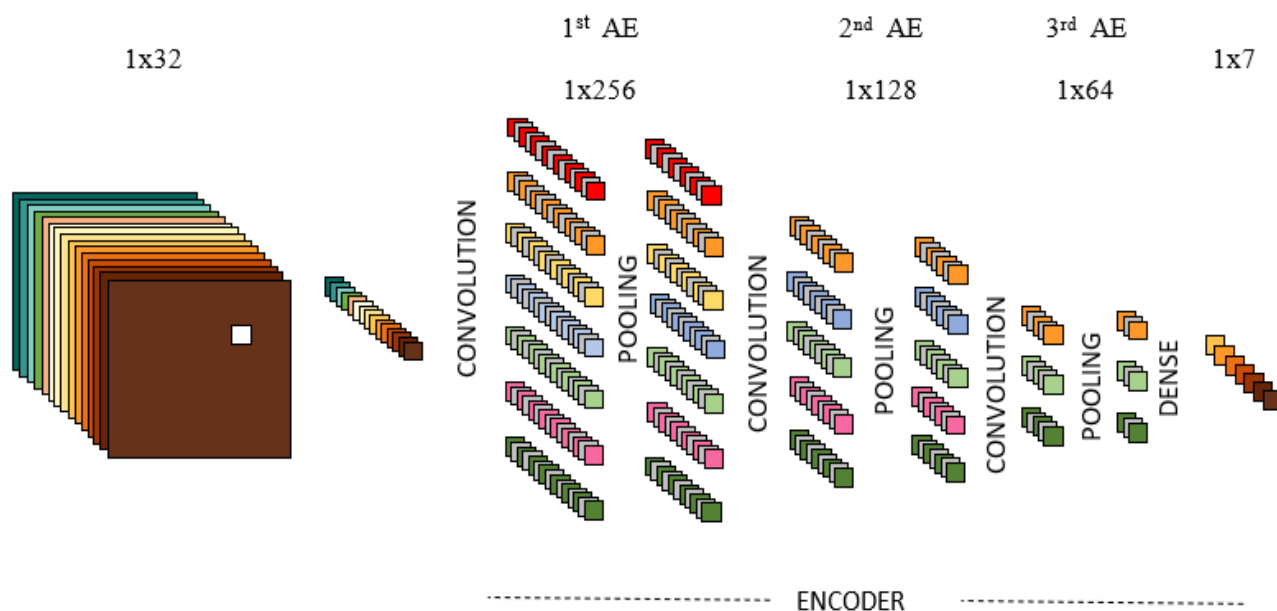

Figure 5 - Proposed SAE Architecture-Encoding phase

The size of the input layer is equal to the number of available bands. For example, 32 bands for the Indian Pines data set (22 clear bands and 10 noisy bands). In each convolutional step, the input data is filtered using 1x3 linear filters, and the ReLU activation function is used to compute the output.

Then, the result is down sampled with a 1x3 kernel and stored in a pooling layer. In the first AE, it is used 256 filters. The second uses 128 and the last one 64.

The output of this net is then used as input of a conventional (dense) neural net to compute a reduced number of neurons in the latent vector. The size of the latent vector was set equal to the number of desired features. For the Indian Pines scene, the latent vector size was seven.

The SAE-1DCNN network is first used to extract relevant features from the samples and a reduced representation of the original data set can be found in the center of the net. So, for the next step, the weights that are obtained in this step are used as start point for the next step: fine-tuning.

The supervised fine-tuning is based on the concept of transfer learning (Bengio, 2012 and Donahue et al., 2014) and consists of adjusting the weights for a desired purpose. In our case, the aim is to identify noisy bands and subsequently for the classification of the samples in the desired classes. The Fine-tuning step uses two fully connected layers.

The output from the previous encoding stage is used as input in the first fully connected layer and passed to the second fully connected layer, with less neurons, that computes the final output using a conventional, dense, layer and the logistic regression based on the Softmax activation function (minimizes classification errors by adjusting the model parameters of a pretrained network), as mentioned Xing et al., 2016, Nogueira et al., 2017.

Figure 6 displays the mechanism of the proposed model based on the two stages mentioned above. In the following subsections it is described the principles of the use of stacked autoencoders and fine tuning and the refinement of this concept by the introduction of the convolutional layers.

As the proposed model is trained to classify pixels according to their digital values in a series of hyperspectral bands, the number of neurons in the output layer is equal to the number of classes.

Table 3 details the parameters of the SAE-1DCNN model proposed for the two hyperspectral images used in this work. This table shows the parameters for the pretraining performed in the first autoencoder stage as well as for the supervised fine-tuning stage.
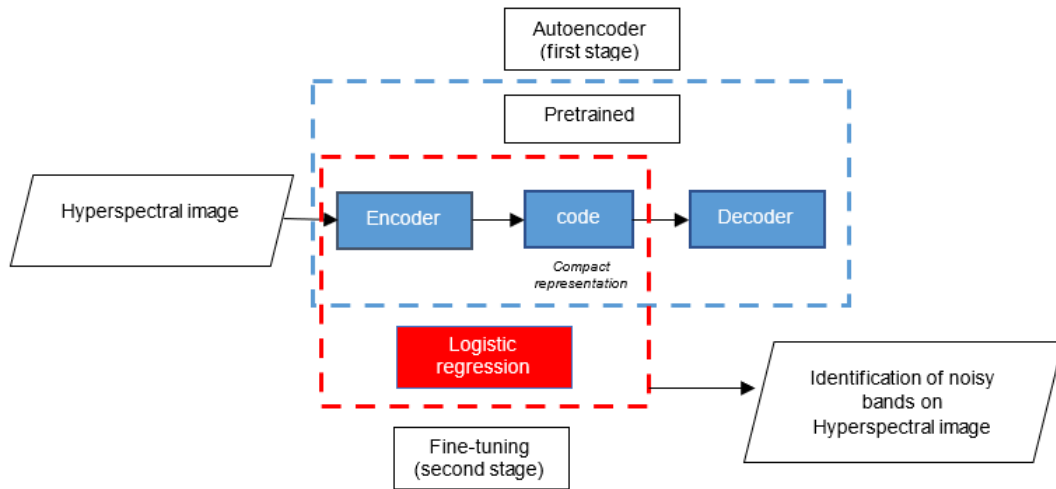

Figure 6 - Global Training Mechanism of the proposed model (SAE-1DCNN)

Table 3 - Information of the architecture of the SAE-1DCNN model for hyperspectral dataset.

<table>
<tr><th colspan="5">SAE-1DCNN proposed method</th></tr>
<tr><th rowspan="3">Hyperspectral dataset</th><th colspan="4">Parameters</th></tr>
<tr><th colspan="2">Pretraining (encoder)</th><th colspan="2">Fine-tuning</th></tr>
<tr><th>Parameters stage</th><th>Filters</th><th>Parameters stage</th><th>Full Connected Neurons</th></tr>
<tr><td rowspan="3">Indian Pines</td><td rowspan="3">Epoch=50;
Optimizer=Adam;
Batch size=32</td><td>256</td><td rowspan="3">Epoch=1500;
Optimizer=Adam;
Learn rate=0.001</td><td>3000</td></tr>
<tr><td>128</td><td>100</td></tr>
<tr><td>64</td><td>7</td></tr>
<tr><td rowspan="3">Salinas</td><td rowspan="3">Epoch=300;
Optimizer=Adam;
Batch size=32</td><td>256</td><td rowspan="3">Epoch=300;
Optimizer=Adam;
Learn rate=0.001</td><td>300</td></tr>
<tr><td>128</td><td>300</td></tr>
<tr><td>64</td><td>16</td></tr>
</table>

Feature selection steps

To evaluate the proposed method (SAE-1DCNN), it was applied to detect noisy bands within an AVIRIS data set. Two image sets were used in the experiments: Salinas and Indian Pines images.

Training samples of different classes were selected in each image, including all bands, and fed into the SAE-1DCNN model. In the hidden layers, a summarized representation of the spectral variation of the pixels was computed, which enables reconstructing the original data. The summarized representation was used to perform image classification, and the accuracy of this result assessed through the kappa used ($kappa_0$). This result was used as reference to measure the loss or gain obtained when a certain band is omitted. The coefficients of the net were frozen, and the model used to classify the same samples, but in each experiment one band was excluded and replaced by a constant value. This was repeated for each spectral band.

The kappa coefficient was computed for each experiment. Next, the experiments were ranked according to the kappa coefficients ($kappa_i$; $i =$ 1, 2, 3,…, number of bands) and the one with the maximal kappa coefficient identified ($kappa_{i\,max}$). In the experiments, one can find kappa values above the first reference kappa ($kappa_0$). Therefore, the reference was adjusted using the maximal kappa computed in the series of experiments. The average between the maximal kappa coefficient ($kappa_{imax}$) and the reference kappa ($kappa_0$) was computed to obtain an adjusted reference kappa ($kappa_{ref}$) as shown in Equation 4. Figure 7 shows the pre-processing methodology by the SAE-1DCNN model for noisy bands detection.

The difference between the adjusted reference kappa ($kappa_{ref}$) and the kappa coefficient of each substitution ($kappa_i$), shown in Equation 5, was used to estimate the contribution of each band. The computed values enable ranking the
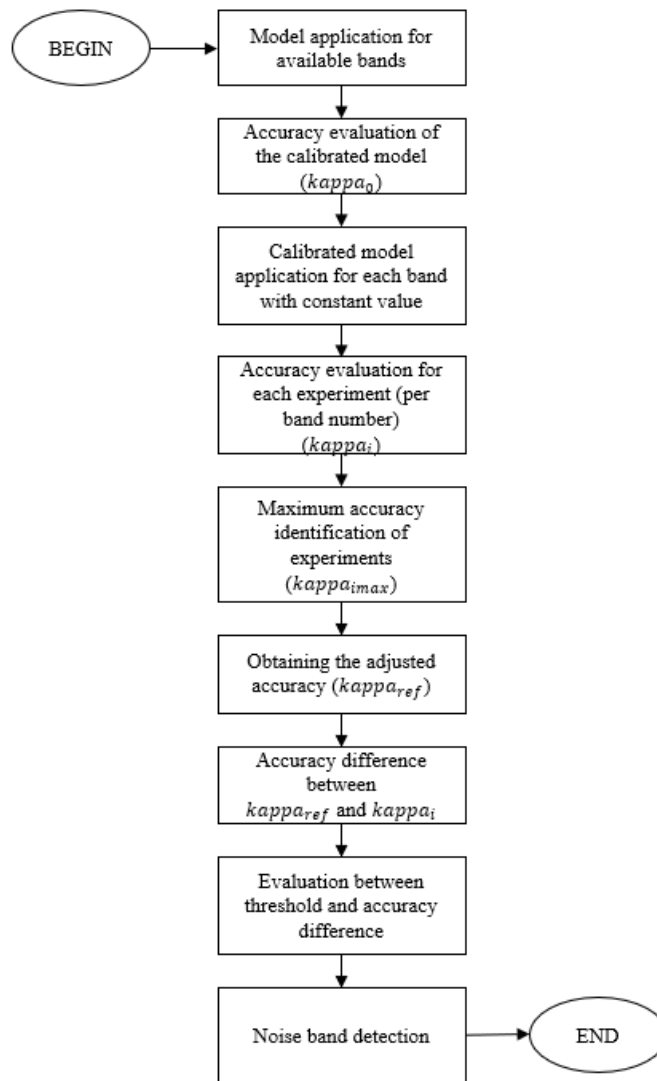
Figure 7 - Methodology for detection of noisy bands step by SAE-1DCNN

experiments from the highest value (high quality) to the lowest (worst quality). Lower values are obtained when a useful band (significant information) is omitted. On the other side, higher values show that the omitted band does not contribute significantly to the classification. Fixing the number of desired bands or applying a threshold enables detecting the bands with less useful information.

As the noisy bands are composed of random pixel values, they are related to high values in equation 5. In the study, a threshold was empirically chosen. If the absolute difference lies below the threshold, then the band can be discarded, as the accuracy of the classification is reduced.

$$kappa_{ref} = 0.5 * (kappa_{i\,max} + kappa_0) \quad (4)$$

$$Dif_i = kappa_{ref} - kappa_i \quad (5)$$

Where,

i: omitted band; $kappa_{ref}$: adjusted reference kappa; $kappa_{i\,max}$: maximal kappa obtained in the experiments omitting one band; $kappa_0$: kappa coefficient of the experiment using all bands.

RESULTS AND DISCUSSION

To detect noisy bands, the first approach was visual inspection of each band. Then, in a second attempt, the SAE-1DCNN model was used to perform the same task.

Noisy Bands Detection

Noisy bands were visually identified and excluded. For this purpose, each band was visualized on the computer screen (detailed in section 2.2.1) and the number of noisy bands was visually estimated. The result of this step depends on the experience of the analyst and different results may be obtained by different

analysts, which is a critic to this method. Nevertheless, it was used as a first approach in the experiments. In a second step, tests were also performed based on the proposed SAE-1DCNN band selection approach.

The bands that were excluded for each hyperspectral image through visual identification are presented in Table 2.

Table 4 - Noisy bands removed by visual identification

Hyperspectral data set	Total bands	Noisy bands	Used
Indian Pines	32	10	22
Salinas	23	5	18

The proposed model was evaluated using AVIRIS hyperspectral images of Indian Pines and Salinas. The SAE-1DCNN band selection method was applied to reduced datasets, with and without noisy bands. For the tests performed in this section (using the SAE-1DCNN model), 18 bands without noise and 5 noisy bands were used in the Salinas experiment. On the other hand, 22 clear bands and 10 noisy bands were used when dealing with the Indian Pines image. This means that 23 bands were used for the Salinas image and 32 bands for the Indian Pines image. For the Salinas image, the noisy bands used were: 108, 111, 159, 160, 162; while for the Indian Pines image: 1, 103, 104, 107, 109, 153, 155, 157, 161, 163. The noisy bands for the two evaluated scenes were randomly chosen, based on the visual analysis, and belong to the red regions and infrared of the electromagnetic spectrum.

In the next step, the experiment was repeated replacing the information of one band by a constant value, which means that this band has no relevant information. Then, the quality of the thematic map of each experiment was analyzed using kappa coefficient. The thresholds of 10% for the Salinas data set and 3% for the Indian

Pines data set were used to identify the bands that do not contribute significantly to the solution. The adjusted reference kappa ($kappa_{ref}$) computed and used for the Salinas image was 88% while for the Indian Pines image it was 76%.

The evaluation and identification of noisy bands was carried out based on the difference between the adjusted reference kappa ($kappa_{ref}$) and the kappa coefficient of each experiment. These differences were compared through the threshold established for each image. Thus, if the difference between these two kappa values is less than the set threshold, it is identified as a noisy band, as shown in Tables 5, 6.

Tables 5 and 6 show the results obtained in the images of Salinas and Indian Pines for the identification of noisy bands. However, 10 and 14 results for Salinas and Indian Pines, respectively, were placed in those tables as a sample of the totality of results obtained in this work. Based on the results obtained in each scene, all the noisy bands used in this section were identified, therefore, they can be eliminated since they do not contribute to improve the classification.

Table 5 - Identification of noisy bands removed by SAE-1DCNN model for Salinas data set.

Model	Number of bands		$kappa_{ref}$	Dif_i
	18 bands		87.55	
	23 bands	18 without noise + 5 noisy bands	87.40	
		108*	89.31	1.31
		111*	89.30	1.30
		159*	89.31	1.31
SAE-1DCNN		160*	89.32	1.32
		162*	89.32	1.32
		7**	58.61	29.39
		11**	69.54	18.46
		17**	25.42	62.58
		37**	31.33	56.67
		153*	45.30	42.70

* noisy bands, ** bands without noise

Table 6 - Identification of noisy bands removed by SAE-1DCNN model for Indian Pines data set.

Model	Number of bands		$kappa_{ref}$	Dif_i
	22 bands		76.04	
	32 bands	22 without noise + 10 noisy bands	77.31	
		1*	77.02	1.02
		103*	77.02	1.02
		104*	78.49	2.49
		107*	78.40	2.40
		109*	78.45	2.45
SAE-1DCNN		153*	78.17	2.17
		155*	78.35	2.35
		157*	78.40	2.40
		161*	78.49	2.49
		163*	78.44	2.44
		23**	23.91	52.09
		27**	23.10	52.90
		169**	67.75	8.25
		171**	69.28	6.72

* noisy bands, ** bands without noise

CONCLUSIONS

In this paper, we introduced the SAE-1DCNN model as feature selection method to detect noisy bands on hyperspectral images. This model integrates an unsupervised approach based on SAE and performs supervised training using CNNs and fine-tuning by logistic regression. The proposed model was applied using two hyperspectral images of the AVIRIS sensor that cover mixed agricultural areas, which allowed evaluating its performance and determining that it is a valid option to perform feature selection for noisy band detection purposes.

The SAE-1DCNN proposed model enables detecting the most significant input variables, in that sense, to identify the bands that affect more significantly the quality of the result, and the less significant, those that do not change the result.

The extraction of noisy bands by visual inspection is subjective because it depends on the criteria of each analyst and useful bands can be discarded, while the automatic selection approach selects relevant information through parameters, models, algorithms and procedures using information contained in the original data.

The proposed automatic method can detect noisy bands and cancel them to avoid inconvenience in the classification step. This is useful because it can be used to bypass band selection based on visual analysis of each spectral band.

The results obtained with the SAE-1DCNN model showed effectiveness in identifying noisy bands, thus encouraging to investigate its potential use to perform the pre-processing steps without relying on visual identification.

DECLARATION OF COMPETING INTEREST

The authors declare that they have no known competing financial interests or personal relationships that could have appeared to influence the work reported in this paper.

ACKNOWLEDGEMENTS

REFERENCES

AUDEBERT, N.; LE SAUX, B.; LEFÈVRE, S. Deep learning for classification of hyperspectral data: A comparative review. **IEEE geoscience and remote sensing magazine**, v. 7, n. 2, p. 159-173, 2019.

BANERJEE, B.P.; RAVAL, S.; CULLEN, P.J. UAV-hyperspectral imaging of spectrally complex environments. **International Journal of Remote Sensing**, v. 41, n. 11, p. 4136-4159, 2020.

BENGIO, Y. Deep learning of representations for unsupervised and transfer learning. In: **Proceedings of ICML**, p. 17-36, 2012.

BOOYSEN, R.; JACKISCH, R.; LORENZ, S.; ZIMMERMANN, R.; KIRSCH, M.; NEX, P.A.; GLOAGUEN, R. Detection of REEs with lightweight UAV-based hyperspectral imaging. **Scientific Reports**, v. 10, n. 1, p. 1-12, 2020.

CAO, Q.; YU, G.; SUN, S.; DOU, Y.; LI, H.; QIAO, Z. Monitoring water quality of the Haihe river based on ground-based hyperspectral remote sensing. **Water**, v. 14, n. 1, p. 22, 2021.

CARRINO, T. A.; CRÓSTA, A. P.; TOLEDO, C. L. B.; SILVA,

A. M. Hyperspectral remote sensing applied to mineral exploration in southern Peru: A multiple data integration approach in the Chapi Chiara gold prospect. **International Journal of Applied Earth Observation and Geoinformation**, v. 64, p. 287-300, 2018.

CHENG, G.; HAN, J.; LU, X. Remote sensing image scene classification: Benchmark and state of the art. **Proceedings of the IEEE**, v. 105, n. 10, p. 1865-1883, 2017.

DONAHUE, J.; JIA, Y.; VINYALS, O.; HOFFMAN, J.; ZHANG, N.; TZENG, E.; DARRELL, T. Decaf: A deep convolutional activation feature for generic visual recognition. In INTERNATIONAL CONFERENCE ON MACHINE LEARNING, p. 647-655, 2014.

ETTABAA, K.S. & SALEM, M.B. Adaptive progressive band selection for dimensionality reduction in hyperspectral images. **Journal of the Indian Society of Remote Sensing**, v. 46, n. 2, p. 157-167, 2018.

HUGHES, G.F. On the mean accuracy of statistical pattern recognizers. IEEE Trans. **Inform. Theory IT**, v. 14, p. 55–63, 1968.

ISHIDA, T.; KURIHARA, J.; VIRAY, F.A.; NAMUCO, S.B.; PARINGIT, E.C.; PEREZ, G.J.; TAKAHASHI, Y.; MARCIANO JR, J.J. A novel approach for vegetation classification using UAV-based hyperspectral imaging. **Computers and electronics in agriculture**, v. 144, p. 80-85, 2018.

JACKISCH, R.; MADRIZ, Y.; ZIMMERMANN, R.; PIRTTIJÄRVI, M.; SAARTENOJA, A.; HEINCKE, B.H.; SALMIRINNE, H.; KUJASALO, J.; ANDREANI, L.; GLOAGUEN, R. Drone-borne hyperspectral and magnetic data integration: Otanmäki Fe-Ti-V deposit in Finland. **Remote Sensing,** v. 11, n. 18, p. 2084, 2019.

JIA, S.; JI, Z.; QIAN, Y.; SHEN, L. Unsupervised band selection for hyperspectral imagery classification without manual band removal. **IEEE Journal of Selected Topics in Applied Earth Observations and Remote Sensing**, v. 5, n. 2, p. 531-543, 2012.

LAPORTE-FAURET, Q.; LUBAC, B.; CASTELLE, B.; MICHALET, R.; MARIEU, V.; BOMBRUN, L.; LAUNEAU, P.; GIRAUD, M.; NORMANDIN, C.; ROSEBERY, D. Classification of Atlantic coastal sand dune vegetation using in situ, uav, and airborne hyperspectral data. **Remote Sensing**, v. 12, n. 14, p. 2222, 2020.

LECUN, Y.; BENGIO, Y.; HINTON, G. Deep learning. **Nature**, v. 521, n. 7553, p. 436, 2015.

LU, X.; WANG, Y. & YUAN, Y. Graph-regularized low-rank representation for destriping of hyperspectral images. **IEEE Transactions on Geoscience and Remote Sensing**, v. 51, n. 7, p. 4009-4018, 2013.

MA, L.; LIU, Y.; ZHANG, X.; YE, Y.; YIN, G.; JOHNSON, B.A. Deep learning in remote sensing applications: A meta-analysis and review. **ISPRS journal of photogrammetry and remote sensing**, v. 152, p. 166-177, 2019.

MAFFEI, A.; HAUT, J. M.; PAOLETTI, M. E.; PLAZA, J.; BRUZZONE, L.; PLAZA, **A. A single model CNN for hyperspectral image denoising. IEEE Transactions on Geoscience and Remote Sensing,** v. 58, n. 4, p. 2516-2529, 2019.

MAGGIORI, E.; TARABALKA, Y.; CHARPIAT, G.; ALLIEZ, P. Convolutional neural networks for large-scale remote-sensing image classification. **IEEE Transactions on geoscience and remote sensing**, v. 55, n. 2, p. 645-657, 2016.

MEI, S.; JI, J.; GENG, Y.; ZHANG, Z.; LI, X.; DU, Q. Unsupervised Spatial–Spectral Feature Learning by 3D Convolutional Autoencoder for Hyperspectral Classification. **IEEE Transactions on Geoscience and Remote Sensing**, v. 57, n. 9, p. 6808-6820, 2019.

MINGHELLI, A.; VADAKKE-CHANAT, S.; CHAMI, M.; GUILLAUME, M.; MIGNE, E.; GRILLAS, P.; BOUTRON, O. Estimation of bathymetry and benthic habitat composition from hyperspectral remote sensing data (BIODIVERSITY) using a semi-analytical approach. **Remote Sensing**, v. 13, n. 10, p. 1999, 2021.

NOGUEIRA, K.; PENATTI, O.A.; DOS SANTOS, J.A. Towards better exploiting convolutional neural networks for remote sensing scene classification. **Pattern Recognition**, v. 61, p. 539-556, 2017.

PAOLETTI, M. E.; HAUT, J. M.; PLAZA, J.; PLAZA, A. A new deep convolutional neural network for fast hyperspectral image classification. **ISPRS Journal of Photogrammetry and Remote Sensing**, v. 145, p. 120-147, 2018.

PAOLETTI, M. E.; HAUT, J. M.; PLAZA, J.; PLAZA, A. Deep learning classifiers for hyperspectral imaging: A review. **ISPRS Journal of Photogrammetry and Remote Sensing**, v. 158, p. 279-317, 2019.

PAUL, A. & CHAKI, N. Dimensionality reduction of hyperspectral images using pooling. **Pattern Recognition and Image Analysis**, v. 29, n. 1, p. 72-78. 2019.

PAUL, A.; KUNDU, A.; CHAKI, N.; DUTTA, D.; JHA, C.S. Wavelet enabled convolutional autoencoder based deep neural network for hyperspectral image denoising. **Multimedia tools and applications**, p. 81, n. 2, p. 2529-2555, 2022.

PETSCHARNIG, S.; LUX, M. & CHATZICHRISTOFIS, S. **Dimensionality reduction for image features using deep learning and autoencoders**. In Proceedings of the 15th international workshop on content-based multimedia indexing (pp. 1-6). 2017.

RASTI, B.; SCHEUNDERS, P.; GHAMISI, P.; LICCIARDI, G.; CHANUSSOT, J. **Noise reduction in hyperspectral imagery: Overview and application**. Remote Sensing, v. 10, n. 3, p. 482, 2018.

SERPICO, S. B.; D'INCA, M.; MELGANI, F.; MOSER, G. Comparison of feature reduction techniques for classification of hyperspectral remote sensing data. In: IMAGE AND SIGNAL PROCESSING OF REMOTE SENSING, VIII. **Proceedings** of SPIE, v. 4885, p. 347–358, 2003.

VENKATESH, B. & ANURADHA, J. A review of feature selection and its methods. **Cybernetics and Information Technologies**, v. 19, n. 1, p. 3-26, 2019.

WEI, L.; HUANG, C.; ZHONG, Y.; WANG, Z.; HU, X.; LIN, L. Inland waters suspended solids concentration retrieval based on PSO-LSSVM for UAV-borne hyperspectral remote sensing imagery. **Remote Sensing**, v. 11, n. 12, p. 1455, 2019.

WINDRIM, L.; RAMAKRISHNAN, R.; MELKUMYAN, A.; MURPHY, R. J.; CHLINGARYAN, A. **Unsupervised feature-learning for hyperspectral data with autoencoders. Remote Sensing**, v. 11, n. 7, p. 864, 2019.

XING, C.; MA, L.; YANG, X. Stacked denoise autoencoder based feature extraction and classification for hyperspectral images. **Journal of Sensors**, v. 2016, 2016.

YANG, X.; YE, Y.; LI, X.; LAU, R. Y.; ZHANG, X.; HUANG, X. Hyperspectral image classification with deep learning models. **IEEE Transactions on Geoscience and Remote Sensing**, v. 56, n. 9, p. 5408-5423, 2018.

ZABALZA, J.; REN, J.; ZHENG, J.; ZHAO, H.; QING, C.; YANG, Z.; MARSHALL, S. Novel segmented stacked autoencoder for effective dimensionality reduction and feature extraction in hyperspectral imaging. **Neurocomputing**, v. 185, p. 1-10, 2016.

ZEBARI, R.; ABDULAZEEZ, A.; ZEEBAREE, D.; ZEBARI, D.; SAEED, J. A comprehensive review of dimensionality reduction techniques for feature selection and feature extraction. **Journal of Applied Science and Technology Trends**, v. 1, n. 2, p. 56-70, 2020.

ZHANG, Q.; YUAN, Q.; LI, J.; LIU, X.; SHEN, H.; ZHANG, L. Hybrid noise removal in hyperspectral imagery with a spatial–spectral gradient network. **IEEE Transactions on Geoscience and Remote Sensing**, v. 57, n. 10, p. 7317-7329, 2019.